Acta Cryst. (1977). A33, 987–992

The ω/θ Scan – an Efficient X-ray Monochromation Technique

BY W. A. DENNE

CSIRO, Division of Chemical Physics, PO Box 160, *Clayton, Victoria, Australia* 3168

(*Received* 2 *December* 1976; *accepted* 27 *May* 1977)

It is possible to obtain essentially monochromatic spot profiles with a single-crystal diffractometer by using the specimen crystal as a dispersive element, and by carrying out an ω/θ integration scan with restricted detector slits. An expression for the detector slit width is derived and the technique is tested experimentally. It appears that there is little difficulty in monochromating to $\pm 1\%$ of the nominal X-ray wavelength as a routine procedure. It is also quite straightforward to work with the $K\alpha_1$ line alone for medium and high-angle reflexions. The range of wavelengths detected can be made independent of diffraction angle; integrated intensity errors due to variable spectral response can therefore be effectively eliminated. This technique facilitates a higher and more constant degree of X-ray monochromation than the pyrolytic-graphite monochromator or the solid-state detector.

Introduction

Alexander & Smith (1962) and Denne (1977*a*) (hereafter called D1) have shown the importance of using a constant bandwidth in accurate integrated-intensity measurements. A recent analysis of the single-crystal diffractometer (Denne, 1977*b*, hereafter called D2) has revealed a novel method of monochromation or 'bandwidth control'; this method entails an ω/θ scan with restricted detector slits. This paper describes a detailed assessment of the technique.

Theory

It is shown in D2 that the diffracted beam from a small and reasonably perfect single crystal is essentially a high-resolution X-ray spectrum in the plane of diffraction. The crystal can be used as its own monochromator simply by placing slits in the diffracted beam so that only the desired portion of the X-ray spectrum reaches the detector (Fig. 1). When the crystal rotates, the diffracted beam *from a given point* on the source rotates at *twice the angular velocity of the crystal* and *changes wavelength continuously* (Fig. 2*a*). However, *a given wavelength* in the diffracted beam arises *from a different point on the source at each instant of the scan* and it will rotate at the *same angular velocity* as the crystal (Fig. 2*b*). An ω/θ scan with a given detector aperture therefore maintains a constant bandpass while integrating an X-ray reflexion from a small single crystal.

To correct for the background, *Bremsstrahlung* and harmonic radiation associated with the peak signal it is necessary to take background measurements. This may be done by using the ω/θ scan to measure similar wavelength ranges on either side of the peak bandpass. The undesired signals will vary only slowly over a range of three times the peak bandwidth so that subtraction of the mean background intensity will eliminate these signals from the peak in the usual way. Fig. 3 illustrates this on an experimentally determined Cu $K\alpha$ spectrum. A bandwidth of three times the $K\alpha$ doublet splitting is portrayed. Because of the smaller range of wavelengths detected, background counts are lower than for $\omega/2\theta$ scans. This range can be maintained constant with change in θ by adjusting the detector aperture; low-angle background counts should therefore be similar to those for high-angle scans, and will not display the marked asymmetry which arises at low angles from change in bandwidth (*cf.* Furnas, 1965). The smallness of the detector aperture will also reduce general background and thermal diffuse scattering signals.

The actual X-ray energy range which is detected will be determined by the width of the detector slits. To maintain a given bandpass, the slits must change width with diffraction angle. The slit-width for a perfect point-crystal specimen is found, by differentiating the Bragg equation, to be $R\alpha \tan\theta$, where R is the specimen-to-slit distance and α is the fractional bandpass nominated. As shown in D2, however, the spectral resolution is dependent on the crystal width, w. If the crystal has mosaic structure, the resolution is further reduced by the angular range of mosaic misorientation,

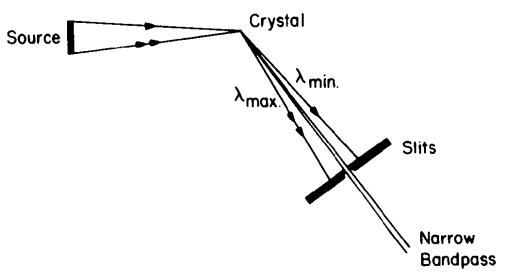

Fig. 1. Monochromation using the specimen crystal as a dispersive element and detector slits to isolate a given bandpass.

η. The expression for the slit-width, W, therefore becomes:

$$W = w + R\eta + R\alpha \tan\theta . \qquad (1)$$

The constant term, $(w + R\eta)$, will cause a small angle-dependent variation in the wavelength range detected. The integrated intensity error incurred was computed for various ratios of $W/R\alpha \tan\theta$ likely to be found in practice. A rectangular function was used to represent the resolving power of the diffractometer, though later this was replaced by a delta function to assess the sensitivity of the results to function shape. Details of the calculations are given in the Appendix. The results are shown in Fig. 4.

It is clear that for a $\pm 1\,\%$ bandwidth the truncation error is less than $1\,\%$ over a very wide range for both Mo and Cu $K\alpha$ radiations. For most purposes this error may be neglected, though it is straightforward to correct intensity data using Fig. 4. The $(w + R\eta)$ term

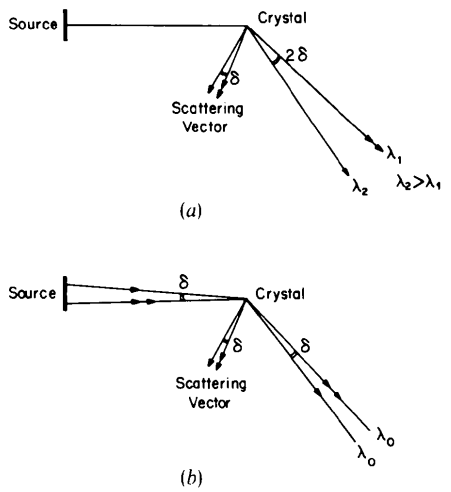

Fig. 2. The effect of crystal rotation on the diffracted beam. (*a*) The diffracted beam from a point on the source rotates at twice the angular velocity of the crystal and changes wavelength continuously. (*b*) A given wavelength in the diffracted beam rotates at the same angular velocity as the crystal.

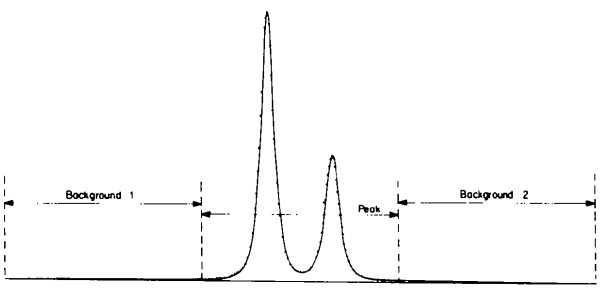

Fig. 3. A Cu $K\alpha$ spectrum using a diamond 400 reflexion, illustrating the peak and background bandpass at a resolution of three times the Cu $K\alpha$ doublet splitting. Note that these will be virtually independent of diffraction angle with an ω/θ scan.

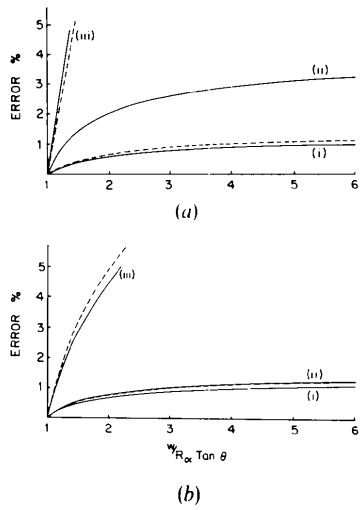

Fig. 4. Truncation errors caused by finite crystal size and mosaic spread presented as a function of $W/R\alpha \tan\theta$. (*a*) Cu $K\alpha$ and (*b*) Mo $K\alpha$ radiation with a bandpass of (i) $\pm 1\,\%$, (ii) 3 times the $K\alpha$ doublet splitting, (iii) 10 times the Cu $K\alpha_1$ line full width at half height. Full lines are calculated with a rectangular resolution function; dotted lines are (i) and (iii) calculated with a delta resolution function.

of equation (1) causes much larger truncation errors when working with the $K\alpha_1$ line alone. Either the high-resolution bandwidth should not be used until $(w + R\eta) \leq (R\alpha \tan\theta)/10$, or corrections should be applied using Fig. 4.

The calculations with a delta resolution function are plotted in Fig. 4 as dotted lines. The results agree well with those using a rectangular function. The truncation corrections must therefore be principally a function of the magnitude of $(w + R\eta)$, or the width of the spectral smearing function, rather than the form of this function. This means that the curves of Fig. 4 will be valid, no matter what the crystal shape or mosaic structure.

Experimental tests

The basic theory was tested by photographing various diffracted beams during integrating scans. Fig. 5 compares the diffracted beam of an α-glycine 020 reflexion during an ω/θ step scan with those of the diamond 111 and 400 reflexions during ω step scans (Cu $K\alpha$ radiation). The film has been raised perpendicular to the diffraction plane after each step to show the detected signal clearly. The collinearity of the characteristic lines for the ω/θ scan shows that a given wavelength rotates at the same angular velocity as the crystal; measurement of the line displacements in the ω-scan photographs confirm this. The high resolution of the spectrum is demonstrated by the clean separation of the Cu $K\alpha$ doublet, even when 2θ is only 15°. The increase in the dispersion with diffraction angle is also quite evident.

Equation (1) was tested by taking a series of diffracted-beam photographs at increasing diffraction angle. Continuous ω/θ scans were used with a 0·4 mm diameter diamond and Mo $K\alpha$ radiation. The films were placed at the detector position and the detector slits were set according to equation (1). The results are shown in Fig. 6. The dispersion is sufficiently low in the first two frames for the film to record the spectral tails and their cut-off by the slits. The slit limits are indicated in successive frames. It is obvious that the same spectral band is accepted at all angles in spite of the increase in dispersing power. It is also evident that even with such a large crystal, it is possible to work with the $K\alpha_1$ line alone from as low a diffraction angle as $\theta = 29°$.

To investigate this possibility, three of these reflexions were measured using an ω/θ scan with both a $K\alpha$ doublet and $K\alpha_1$ bandpass. The ratios of these integrated intensities are shown in Table 1, together with their estimated standard deviations. The values have been corrected for truncation using the curves in Fig. 4; the results obtained agree to within experimental error. The mean ratio is in excellent agreement with that predicted from spectroscopic data (Dyson, 1973), thus indicating the effectiveness of the technique and validating the curves of Fig. 4. The mean intensity ratio of Table 1 is required for the relative scaling of integrated intensities measured with the two different bandwidths. Although an e.s.d. of 0·3% may not be sufficiently small for work of the highest accuracy, the average of more measurements may be taken or the theoretical value selected. Note that the ratio obtained is independent of the specimen crystal and of the extinction or absorption in the measured reflexions.

Table 1. *Relative intensities of reflexions measured with a bandpass of three times the $K\alpha$ doublet and* 10 *times the $K\alpha_1$ full width at half height*

Mo radiation; intensities corrected according to Fig. 4; theoretical value based on spectroscopic data from Dyson (1973); e.s.d.'s in parentheses.

hkl	$I\alpha_1/I\alpha_1\alpha_2$ ratio
355	0·621 (0·008)
533	0·617 (0·008)
422	0·606 (0·004)
Mean	0·613 (0·003)
Theoretical value	0·619

Table 2 shows a detailed comparison of some intensities measured by $\omega/2\theta$ and ω/θ scans, with Mo $K\alpha$ radiation and bandwidths of three times the $K\alpha$ doublet splitting ($\pm 0{\cdot}006$ Å or ± 170 eV) and 10 times the $K\alpha_1$ full width at half height ($\pm 0{\cdot}001$ Å or ± 30 eV). The background signals for the ω/θ $K\alpha$ doublet scans are a constant fraction of the peak intensity, as anticipated from the theory, and are also lower than for the corresponding $\omega/2\theta$ scan. The $\omega/2\theta$ background signals increase with decreasing diffraction angle because of the increase in effective bandwidth. The ω/θ background signals with $K\alpha_1$ bandpass are lower than for both the other scans because the resolution is so much higher. Note the high background for the 555 and 933 reflexions for both the ω/θ and $\omega/2\theta$ scans; this is due to harmonic radiation. With the same scan rate, the integrated intensity e.s.d. values for the $K\alpha_1$ measurements are similar to those for the $\omega/2\theta$ scans, in spite of a 40% reduction in scan time as well as a 33% loss in signal due to the elimination of the $K\alpha_2$ line.

Diamonds are fairly perfect crystals and since the routine application of this technique depends on obtaining specimens of adequate perfection, the low-angle diffracted beams from eight crystals were photographed so that the perfection of typical specimens could be assessed. The crystals tested were specimens which had been used for structure analysis in this laboratory over a period of years. The results showed that all except one were sufficiently perfect for monochromation to ± 1%. The crystal that formed the exception was cut from a soft needle; no doubt, with more care, a better specimen could have been prepared. A little care was taken in preparing a sodium chloride crystal, which may be considered the archetype of

Table 2. *The background/peak ratio* (Bg/Pk) ($\times 10^3$), *counting statistical e.s.d. in integrated intensity* ($\times 10^3$) *and relative scan time for $\omega/2\theta$ and ω/θ measurements of some diamond reflexions with* Mo $K\alpha$ *radiation*

Ranges used were ($2° + \alpha_1,\alpha_2$ separation) for $\omega/2\theta$ scans; $3 \times \alpha_1,\alpha_2$ separation ($\pm 0{\cdot}006$ Å or ± 170 eV) and $10 \times$ Mo $K\alpha_1$ full width at half height (FWHH) ($\pm 0{\cdot}001$ Å or ± 30 eV) for the ω/θ scans.

Reflexion		$\omega/2\theta$ Range $= 2° + \alpha_1\alpha_2$ splitting		ω/θ Range $= 3 \times \alpha_1\alpha_2$ splitting			ω/θ Range $= 10 \times \alpha_1$ FWHH		
hkl	2θ (°)	Bg/Pk	e.s.d. (fractional)	Bg/Pk	e.s.d. (fractional)	time saved	Bg/Pk	e.s.d. (fractional)	time saved
111	19·87	149	3	56	3	27%			
311	38·59	88	3	50	3	8%			
422	58·43	64	3	50	3	−10%	20	4	42%
533	81·58	57	6	58	5	−38%	20	7	42%
355	99·86	61	7	74	7	−64%	30	9	43%
555	119·27	245	10				189	10	43%
931	143·76	75	7				37	7	45%
933	164·88	223	9				88	5	31%

mosaic specimens (Bragg, James & Bosanquet, 1921). Clear $K\alpha_1$–$K\alpha_2$ splitting at $2\theta = 32°$ indicated that the crystal was sufficiently perfect for use with the present technique.

Practical considerations

1. *Slit mechanisms*

Automatic slit control is available on many computer-controlled diffractometers. For diffractometers without this facility, a simple slit mechanism can be constructed using the relative positions of the incident and diffracted beam collimators for drive and control, and such a device has been constructed in this laboratory. A simpler expedient is to use a series of fixed slits. Provided each slit is used only when its width is greater that the W value given by equation (1), Fig. 4 can be used to correct for any truncation errors incurred. For a $\pm 1\%$ bandpass, corrections may not be necessary, as 98·6% and 98·5% respectively of the Cu and Mo $K\alpha$ radiations are detected with this bandwidth. At worst, therefore, too wide a slit can only produce a 1·5% error.

2. *Scan limits*

The integration-scan range for the ω/θ scan is somewhat different from that required for ω and $\omega/2\theta$ scans. Both circles must scan between limits $(W/R+\beta)/2$ on either side of the setting angles which correspond to the centre wavelength of the bandpass being measured. (β is the angle subtended by the source at the crystal.) Note that for a finite mosaic crystal, an effective bandwidth of $W/R \tan\theta$ must be used for calculating the centre wavelength of the background scans. Note also that, for work with the $K\alpha_1$ line alone, only a low-angle background may be taken, as the high-angle background will contain a substantial amount of the $K\alpha_2$ line.

The values of w, η and β may be determined from diffracted-beam photographs (see D2) or from diffractometer ω scans using very fine detector slits.

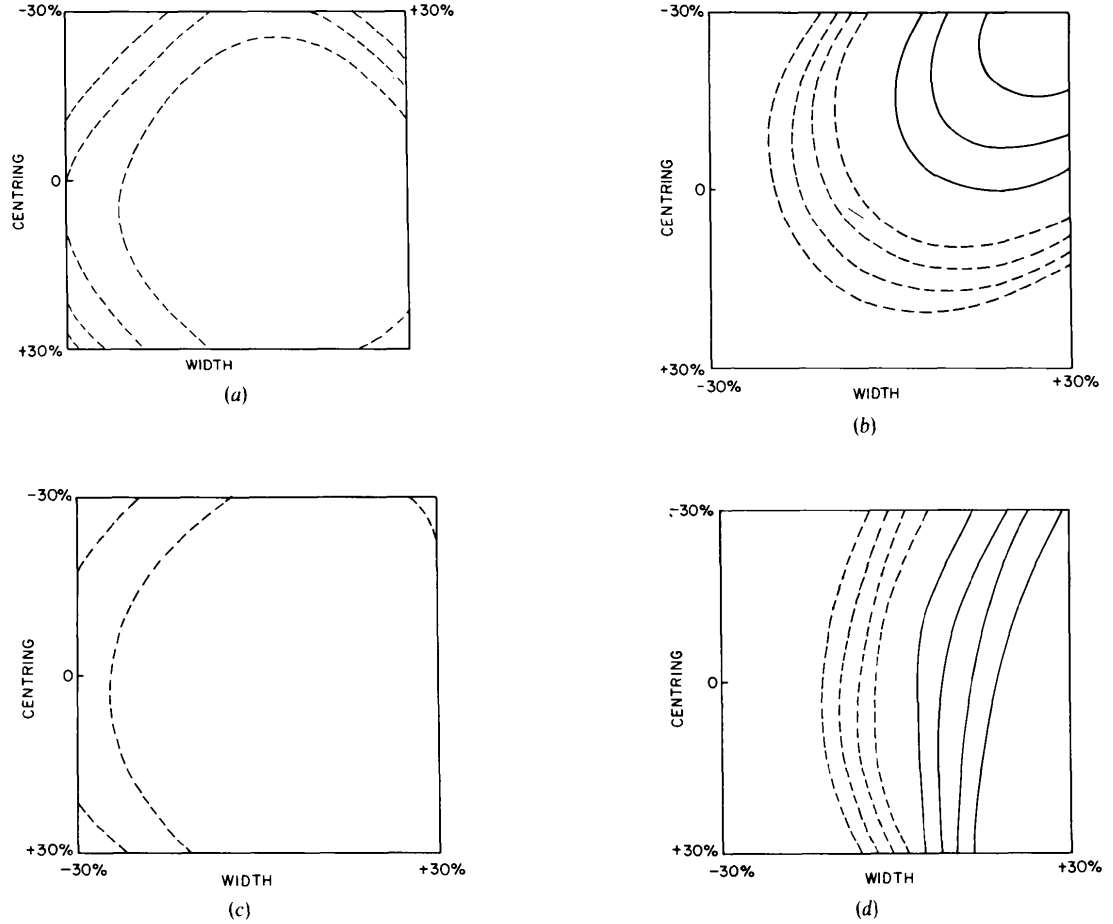

Fig. 7. The effect of slit width and centring errors on integrated intensity expressed in terms of the nominal slit width. (*a*) Mo $K\alpha$ $\pm 1\%$ bandpass. (*b*) Mo $K\alpha_1$, 10 times full width at half height. (*c*) Cu $K\alpha$ $\pm 1\%$. (*d*) Cu $K\alpha_1$, 10 times the full width at half height. Contours at $\pm 0{\cdot}25\%$, $\pm 0{\cdot}5\%$, $\pm 0{\cdot}75\%$, $\pm 1\%$, error. (Dotted contours are negative.)

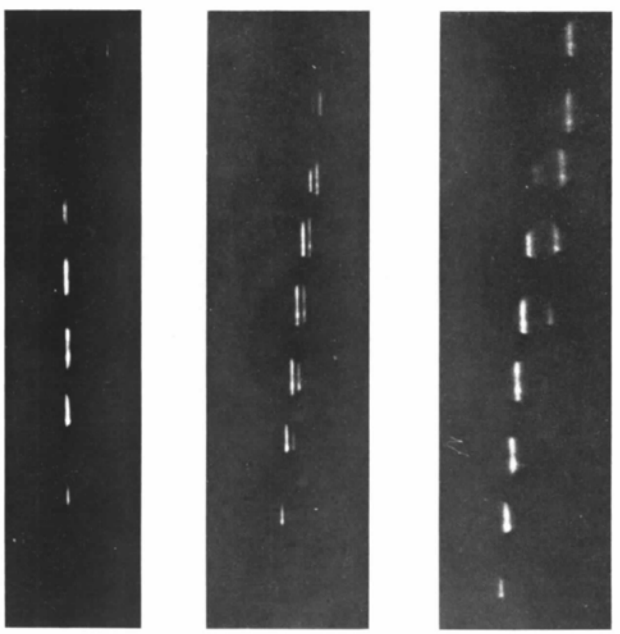

(*a*) (*b*) (*c*)

Fig. 5. Photographs of diffracted beams during step scans. (Film raised vertically after each step for the sake of clarity.) (*a*) ω/θ scan; α-glycine 020 reflexion; $2\theta=15°$. (*b*) ω scan; diamond 111 reflexion; $2\theta=44°$. (*c*) ω scan; diamond 400 reflexion; $2\theta=120°$. Cu $K\alpha$ radiation used for all three scans, (0·05° steps).

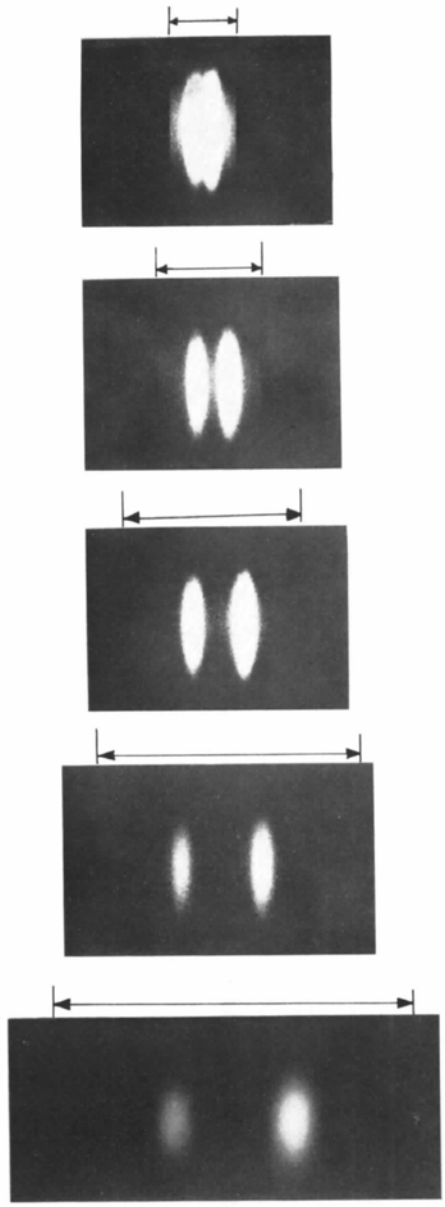

(*a*)

(*b*)

(*c*)

(*d*)

(*e*)

Fig. 6. Photographs of the detector input for various diamond reflexions with the ω/θ scan, and a bandpass of three times the $K\alpha$ doublet splitting of the Mo K radiation. (28 cm crystal-to-slit distance). (*a*) 111 reflexion; $2\theta=19°$. (*b*) 311 reflexion; $2\theta=38°$. (*c*) 422 reflexion; $2\theta=58°$. (*d*) 533 reflexion; $2\theta=81°$. (*e*) 355 reflexion; $2\theta=100°$.

[*To face p.* 990

3. *Slit width and centring tolerances*

With the methods outlined in the Appendix, integrated-intensity errors have been computed for various slit-width and slit-centring errors. The results are plotted as a percentage of the nominal slit width in the contour maps of Fig. 7. It is evident that for a 0·5% error in integrated intensity, the setting tolerance is ±30% for a ±1% bandwidth, ±10% for a bandwidth of 10 times the Mo $K\alpha_1$ line width and ±5% for a bandwidth of 10 times the Cu $K\alpha_1$ line width. The calculations were performed for a perfect point crystal, as this case is the most sensitive to slit-setting errors.

With a ±1% bandwidth and a setting reliability assumed equivalent to an angle of 0·05° at the crystal, integrated intensities may be measured to an accuracy of 0·5% from $\theta=8{\cdot}3°$. To measure reflexions with smaller θ values to the same accuracy, it is desirable to maintain the minimum slit width of ±0·083° and apply corrections from Fig. 4 if necessary.

The tolerances for work with the $K\alpha_1$ line are more stringent. However, if a setting reliability equivalent to an angle of 0·02° at the crystal is assumed, integrated-intensity measurements may be carried out with an accuracy of 0·5% from $\theta=30°$ for Mo $K\alpha_1$ (with a minimum slit width of 0·2°) and from $\theta=63°$ for Cu $K\alpha_1$ (with a minimum slit width of 0·4°). Truncation corrections from Fig. 4 must be applied unless $(w+R\eta)\leq (R\alpha\tan\theta)/10$.

4. *Stability*

It is obviously essential to have a crystal mounting and goniometer head which are both stable to better than 0·01° over extended periods of time if centring errors are to be avoided. However, such stability can easily be obtained if due care is exercised (*e.g.* Denne, 1971*a*, *b*).

Conclusions

It is practicable to use the ω/θ scan coupled with restricted detector slits to monochromate the diffracted beams from a single-crystal diffractometer. A bandpass of ±1% of the Cu and Mo nominal $K\alpha$ wavelengths may be attained as a routine procedure. A bandpass to 10 times the $K\alpha_1$ line width can be used over a wide range of diffraction angles. In both cases the integrated-intensity error due to variable spectral response may be reduced to less than 0·5%. This degree of monochromation effectively eliminates truncation errors (D1), and reduces errors arising from asymmetric and variable backgrounds (Young, 1961; Furnas, 1965). The technique reduces background count rates and scan times, thereby increasing statistical accuracy. The reduction in detector aperture reduces thermal diffuse scattering signals, especially in the high-angle region where the signals are strongest.

The ω/θ scan performs considerably better than the pyrolytic graphite monochromator (Denne, 1977*c*), both in the degree of monochromation and the constancy with which it is maintained. There is also no loss of flux, no complications with beam inhomogeneity, nor uncertain polarization factors. The performance of this technique is also superior to solid-state detectors. A higher resolution is attainable, and the linearity of the counting-rate is independent of resolution.

APPENDIX

The calculation of truncation corrections for ω/θ scans using a finite crystal with mosaic structure

The width of X-ray lines arises principally from the rapid decay of a K state. The line shape may therefore be regarded as Lorentzian (*cf.* Heitler, 1957; Ladell, Parrish & Taylor, 1959; Denne, 1977*a*). The equation for a Lorentzian line profile is:

$$L(\nu)=\left(\frac{\Delta\nu}{2\pi}\right)\frac{1}{(\nu-\nu_0)^2+(\Delta\nu/2)^2} \qquad (2)$$

and the integral of this function over the frequency range from a to b is:

$$I(a,b)=[\tan^{-1}\{2(\nu-\nu_0)/\Delta\nu\}]_b^a . \qquad (3)$$

With the use of equation (3) and X-ray spectroscopic data from Dyson (1973), it is straightforward to evaluate the fraction of a characteristic X-ray line which is detected by a given bandwidth for both peak and background scans.

For finite crystals with mosaic structure, the situation is more complex. The diffracted beam is no longer a high-resolution spectrum, but is convoluted with a smearing function, $S(\theta)$. The form of $S(\theta)$ has been described in some detail in D2. The limits of the integral in equation (3) must now be extended to the desired bandwidth plus the width of $S(\theta)$. The fraction of a characteristic X-ray line which is detected by a given bandwidth now becomes:

$$I(a,b,\theta_1,\theta_2)=\int_{\theta_1}^{\theta_2} S(\theta)\int_{a+\nu(\theta)}^{b+\nu(\theta_2-\theta_1+\theta)} L(\nu)\,d\nu\,d\theta , \qquad (4)$$

which can be easily evaluated numerically.

The integration of equation (4) has been performed for both peak and background scans with rectangular $S(\theta)$ functions of varying widths. The results are plotted in Fig. 4 as the percentage change in integrated intensity caused by the finite width and mosaic structure of the crystal. These curves are therefore a measure of the truncation error arising from this source.

Since the form of $S(\theta)$ will vary from crystal to crystal and even from one orientation of the same crystal to the next, these calculations were repeated using the same integration limits but with a delta function for $S(\theta)$. The results of this calculation are presented in Fig. 4 as dotted lines; the good agreement of the two sets of results shows that the integrated intensity error depends on the width of the smearing function but is essentially independent of its form.

References

ALEXANDER, L. E. & SMITH, G. S. (1962). *Acta Cryst.* **15**, 983–1004.
BRAGG, W. L., JAMES, R. W. & BOSANQUET, C. H. (1921). *Phil. Mag.* **41**, 309.
DENNE, W. A. (1971*a*). *J. Appl. Cryst.* **4**, 400.
DENNE, W. A. (1971*b*). *J. Appl. Cryst.* **4**, 60–66.
DENNE, W. A. (1977*a*). *Acta Cryst.* A**33**, 438–440.
DENNE, W. A. (1977*b*). *J. Appl. Cryst.* To be published.
DENNE, W. A. (1977*c*). Unpublished.
DYSON, N. A. (1973). *X-rays in Atomic and Nuclear Physics*, pp. 83, 129, London: Longman.
FURNAS, T. C. JR (1965). *Trans. Amer. Cryst. Assoc.* **1**, 67–85.
HEITLER, W. (1957). *The Quantum Theory of Radiation*, pp. 181–188. Oxford Univ. Press.
LADELL, J., PARRISH, W. & TAYLOR, J. (1959). *Acta Cryst.* **12**, 561–570.
YOUNG, R. A. (1961). Tech. Rep. No. 2, Project No. A-389, Office of Naval Research, Washington 25, DC.

Acta Cryst. (1977). A**33**, 992–996

Short-Range Order to Long-Range Order Transition in Rare-Earth Metal Oxide Thin Crystals

BY V. K. KAUL AND U. SAXENA

Department of Physics, Banaras Hindu University, Varanasi-221005, *India*

(*Received* 28 *March* 1977; *accepted* 1 *June* 1977)

The rare-earth metal oxides are known to exhibit several phases which can be either stoichiometric or nonstoichiometric. One such phase which has been recently found to exist in thin-film form corresponds to the monoxide phase *RO*. The oxygen content in this phase, however, has been found to vary such that the phase actually has the stoichiometry RO_x with $1<x<2$. The present paper deals with electron diffraction studies of the SRO → LRO transition in the nonstoichiometric RO_x phase. This transition commences as a result of the creation of oxygen vacancies in the as-grown thin-film phase, when this phase is pulse annealed with an electron beam in the electron microscope, the annealing temperature being about 500 °C. The short-range ordered version is manifested by the appearance of curious diffuse streaks on the diffraction patterns. The diffuse intensity distribution has been found to be situated on a complicated surface (rhombic dodecahedron) in the reciprocal space of the initial f.c.c. phase with $a=5{\cdot}09\pm 0{\cdot}05$ Å and $5{\cdot}37\pm 0{\cdot}05$ Å for erbium and dysprosium oxides respectively. On further pulse annealing at a higher temperature (~900 °C), the short-range ordered version yields to give rise to a long-range ordered superlattice phase which corresponds to the bulk-like b.c.c. phase with $a=10{\cdot}41\pm 0{\cdot}05$ Å and $10{\cdot}18\pm 0{\cdot}05$ Å for erbium and dysprosium oxides respectively. The SRO → LRO transition has also been analysed in terms of the stoichiometric variations resulting from the pulse annealing.

Introduction

Solid-state materials with possible applications have aroused considerable attention, and a large amount of work has been done on them in the recent past. Rare-earth metal oxides form one such class of materials. These are materials capable of being used at high temperatures and have been found to possess interesting dielectric and semiconducting properties (Alper, 1970; Murr, 1967; Tsutsumi, 1970). These oxides, both in bulk and thin-film forms have been found to possess several structural phases (Murr, 1967; Eyring & Holmberg, 1963; Roth & Schneider, 1960; Eick, Baenzigner & Eyring, 1956; Bist, Kumar & Srivastava, 1972). These structural variants exhibit several stoichiometric variations, ranging from the simplicity of the R_2O_3 (R=rare earth metal) phase, whose crystallographic characterization is well established, through the monoxide phase *RO*, which is reasonably well understood, to the rather complicated nonstoichiometric variants, where much less is known in regard to both their existence and the structural details (Murr, 1967; Eick *et al.*, 1956; Bist *et al.*, 1972; Semiltov, Imamov, Ragimli & Man, 1976; Saxena & Srivastava, 1976, 1977; Kaul & Srivastava, 1976). Also, not much work is available relating to the solid-state transformations between one stoichiometric phase and another. Since the physical properties are phase dependent (Murr, 1967; Saxena & Srivastava, 1976), studies involving details of the stability and structural transformations are of obvious importance and need to be looked further into. The present paper deals with an interesting type of transformation in rare-earth metal oxide thin films, particularly those of erbium and dysprosium where the initial and the final phases exhibit long-range order (LRO), these phases being f.c.c. and b.c.c. respectively. The transformation, however, proceeds through an intermediate phase showing short-range order (SRO), which is displayed by the appearance of the diffuse intensity distribution on the diffraction patterns. In passing, it may be mentioned that this type of transformation has recently been reported in the case of In_2Te_3 and the chalcogenides of niobium and molybdenum (Bleris, Karakostas, Stoemensons &